Iranian Journal of Materials Forming 13 (1) (2026) 59-70

Online ISSN: 2383-0042

IJMF

Iranian Journal of Materials Forming

Journal Homepage: http://ijmf.shirazu.ac.ir

Research Article

Uniaxial Compression Behavior of Ni-Open-Cell Structure Depending on the Electroforming Mass and Thickness

Javad Arta[1], Behrad Yaghobzadeh[2], Salar Rohani Nejad[1] and Seyed Mohammad Hossein Mirbagheri[2*]

[1] Expert Engineering, Rahyaft Advanced Sciences & Technologies knowledge-based company, Tehran, Iran
[2] Material Science and Metallurgical Engineering, Amirkabir University of Technology, Tehran, Iran

ARTICLE INFO

Article history:

Received: 28 September 2025
Reviewed: 25 October 2025
Revised: 30 October 2025
Accepted: 8 November 2025

Keywords:

Open-cell structure
Energy absorption
Electroforming
Compression test
Nickel

Please cite this article as:

Arta, J., Yaghobzadeh, B., Rohani Nejad, S. & Mirbagheri, S. M. H. (2026). Uniaxial compression behavior of Ni-open-cell structure depending on the electroforming mass and thickness. *Iranian Journal of Materials Forming*, *13*(1), 59-70. https://doi.org/10.22099/IJMF.2025.54398.1352

ABSTRACT

In this investigation, a series of nickel open-cell structures with cubic geometry were fabricated by electroforming onto stereolithography (SLA) resin 3D-printed templates. The thickness of the electroformed Ni foams was controlled under constant voltage conditions for two days in a warm nickel sulfamate bath. Ni open-cell samples with varying thicknesses and masses were subsequently subjected to uniaxial compression tests, and their deformation behavior was analyzed and modeled using load–displacement curves. The results show that the mass and apparent density of the Ni open-cell samples exhibit a linear relationship with electroforming time at 6 PPI, unlike the Ni thickness. However, the first maximum compressive strength of the samples, measured according to ISO 13314, does not show a linear dependence on thickness. In this work, Ni open-cell foams were successfully fabricated by warm electroforming under controlled temperature and voltage, achieving densities below 0.93 g/cm³, compressive strengths above 7.50 MPa, and energy absorption values exceeding 4.90 J/cm³. These outstanding mechanical properties, particularly the strength-to-density and energy-absorption-to-density ratios at 6 PPI, demonstrate significant potential for advancing the production of nickel open-cell foams.

1. Introduction

Lightweight geometry can be combined with desired stiffness and energy-absorption capacity in metallic lattice structures and foams [1–3]. Periodic open-cell lattices can achieve remarkable stiffness-to-weight ratios [4], and metal foams are being extensively investigated for applications such as battery electrodes and thermal management. The low density and high electrical conductivity of nickel foams, in particular, have attracted considerable attention. For instance, Ni open-

* Corresponding author
E-mail address: Smhmirbagheri@aut.ac.ir (S. M. H. Mirbagheri)
https://doi.org/10.22099/IJMF.2025.54398.1352

cell foams are lightweight battery current collectors, but they need sufficient compressive and tensile strength to withstand handling and processing [5, 6]. According to Gibson-Ashby models, foam strength and modulus increase sharply with relative density [6–8]. Badiche et al. [6] reported that the elastic modulus, compression yield, and tensile fracture stress all follow the Gibson–Ashby scaling laws in low-density Ni foams (relative density ~0.01–0.05). Similarly, Aly et al. [9] measured tensile strength of approximately 0.6 to 0.7 MPa in open-cell Ni foams. Electroformed Ni lattices with a density of 0.9 g/cm^3 and porosity of 84% have also demonstrated compressive yield strengths in the few MPa range (e.g. ~1.8 MPa for heavily plated, heat-treated samples) [5]. These Ni foams exhibit a high energy absorption capacity per mass unit [10].

Ni open-cell foams have been created using various techniques. A common method is to apply metal to a polymer template (such as PU foam or a 3D-printed scaffold), followed by polymer removal. For example, Arnet et al. 3D-printed a polymer scaffold (HIPS), applied a thin conductive coating, electrodeposited Ni (~5–30 μm thickness) and dissolved the polymer. This resulted in Ni foams with a surface area of approximately 46 m^2/kg and porosities exceeding 92% [11]. Similarly, conventional techniques employ reticulated PU foams coated with Ni via CVD or plating; the polymer is then burned out (for example, at 800 °C) to produce a Ni foam [11]. To enable consistent electroplating, the polymer surface must first be metallized (for example, by applying a silver or Ni–P electroless seed layer). The recent study by He et al. illustrates this method: Cu was electroplated (~40 μm) onto the metalized framework after vat-photopolymerized lattices were seed-coated with electroless Ni–P. The lattice's stiffness and compressive strength were significantly enhanced by the thick Cu/Ni shell [12].

The microstructure and mechanical characteristics of the Ni deposit are significantly influenced by the electroplating parameters. Grain size, stress, hardness, and ductility of the Ni coating are controlled by bath chemistry, current density, and additives, according to Thompson et al.'s review of plating onto polymers [13]. Improper parameters can result in high tensile stress and brittleness, while the addition of stress-relieving agents (such as saccharin) can cause compressive stress and increase hardness [13]. Another important factor is surface preparation: since polymers are nonconductive, Ni electrodeposition requires a conductive primer, such as silver paint or electroless metal coating [13]. These elements affect the electroformed lattice's strength and effective stiffness.

These effects are demonstrated by recent work on foam or 3D-printed Ni lattices. Significant strength increases were observed when Rohani Nejad et al. electroformed Ni (and Cu) shells on TPU polymer lattices. In one instance, a Ni-coated lattice showed a peak compressive yield strength of 4.55 MPa, which is about 1.3 × higher than that of the same lattice with a Cu–Ni multilayer shell. It also absorbed about six times more energy than the bare polymer [10]. Thus, the high specific strength (MPa per g/cm^3) and energy-absorption per unit weight of these Ni-coated lattices validate the importance of metalizing 3D-printed structures. Similarly, Shajari et al. plated Ni foams on PU templates and found that a 12-hour plating process (plus heat treatment) produced a compressive strength of approximately 1.84 MPa [5]. According to these studies, energy absorption is improved by shifting deformation from brittle ligament breakage to ductile strut bending through thicker Ni layers and careful plating conditions.

In conclusion, polymer lattices (whether PU or additively manufactured) can be coated with electrodeposited Ni to create open-cell Ni structures [11]. Ni thickness and lattice topology both affect mechanical performance. Ni shells significantly increase lattice strength and toughness, according to numerous studies [10, 12]. Important factors that determine the density and ligament dimensions of the foam are the relative density (foam porosity) and the thickness of the Ni deposit [10, 12]. According to earlier reports, highly porous Ni foams exhibit compressive strengths of a few MPa [5, 14, 15]. The goal of this work is to clarify how deposit thickness adjusts strength and energy absorption in these lightweight materials by varying the

electroforming thickness on 3D-printed Ni lattices and measuring the resulting changes in uniaxial compressive response from brittle fracture to ductile deformation such as a spring.

2. Experimental Method

2.1. Desing and fabrication

In this investigation, Ni open-cell structures were fabricated using the procedure illustrated in Fig. 1. The process consisted of the following steps:

1. Designing a 3D rectangular cubic model with dimensions of 25 × 25 × 40 mm³ using CAD/CAM software (e.g., SolidWorks).
2. Generating a 3D network solid based on the model, with a ligament diameter of 250 µm and 6 PPI, using Rhino/Grasshopper software.
3. Printing the 3D network solid by additive manufacturing of polymeric resins to obtain a resin-based open-cell sample.
4. Depositing a conductive surface layer on the resin-based open-cell sample (6 PPI) by silver electroless plating.
5. Electroforming nickel onto the metallized resin-based open-cell samples in a heated sulfamate electrolyte bath under the conditions given in Table 1: temperature 60 ± 5 °C, pH 4.10 ± 0.20, cathodic current density 5.1–5.4 A/dm², and specific gravity 1.50.

The 3D network solids were converted into G-code using Anycubic Photon Workshop software and printed with an Anycubic Photon M3 Max SLA printer under 380–405 nm UV light, using 210 mL of standard washable liquid resin. More than 20 Ni open-cell samples were electroformed for 44 h at 60 °C.

Table 1. Datasheet of the nickel electroforming solution

Materials name	Values
Nickel sulfamate solution 60% (mL/L)	280
Nickel chloride 6H2O (g/L)	10
Total nickel concentration (g/L)	50
Boric acid (g/L)	33
Pure nickel anodes (wt.%)	99.97

During the electroforming process, one sample was removed from the tank every 2 hours, washed, dried and then weighed. Among the collected samples, those without visible defects were selected based on visual inspection at electroforming times of 8, 14, 22, 28, 32, 34 and 42 hours, respectively. The samples were labled with the prefix *Ni* followed by two digits, indicating the electroforming duration in hours. The weight, density and other necessary data for these samples are summarized in Table 2. From these, samples Ni8, Ni22, Ni32, and Ni 42 were selected for uniaxial compression testing as shown in Fig. 2.

The compression tests were conducted in accordance with the ISO 13314 standard [16] for porous metallic materials. The Instron machine with a 5-ton capacity was used at a displacement rate of 0.1 mm/s (2.5×10^{-3} S^{-1} strain rate) to evaluate the compressive behavior of the Ni open-cell samples at 25 °C temperature. Microstructural images were obtained using an optical microscope.

In this study, the experimental tests were designed to shift the plastic deformation behavior of the nickel open-cell network away from ligament crushing and fracture. By controlling the nickel open-cell structure thickness during warm electroforming, the deformation mode was adjusted from brittle crushing of the metal network to ductile crumpling, with minimal or no crushing. Consequently, the ductile crumpling of the nickel open-cell network enhanced its energy absorption capacity, thereby promoting its application in energy-absorption systems. This claim is further substantiated by the experimental results presented in the following sections.

2.2. Compression behavior of the metallic network

The compression response of the nickel open-cell network under uniaxial loading, corresponding to the Ni open-cell samples shown in Fig. 2, is presented in Figs. 3–6. The deformation behavior of the Ni8 samples (Fig. 3) reveals pronounced crushing and crumpling, associated with ligament collapse of the metallic network, occurring after approximately 20% strain (Fig. 3(d–i)). In contrast, in the samples shown in Fig. 4, crumpling is less pronounced and initiates at a higher strain level of about 30% (Fig. 4(e–i)). Notably, in the cases illustrated in Figs. 5 and 6, particle crushing and ligament collapse are no longer observed.

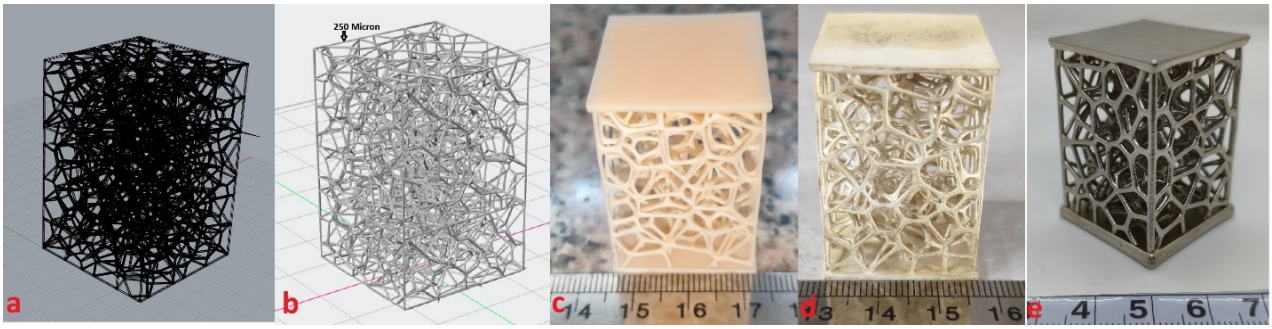

Fig. 1. Sequential steps for producing a Ni open-cell structure with 6 PPI: (a) virtual design, (b) network solid, (c) resin 3D print via SLA, (d) silver metallization, and (e) Ni open-cell sample obtained by electroforming.

Table 2. Properties of Ni open-cell after electroforming

Sample name /properties	Ni8	Ni14	Ni22	Ni28	Ni32	Ni34	Ni42	Ni0
Time electroforms (h)	8	14	22	28	32	34	42	0
Mass (g)	8.40	10.49	13.88	15.22	19.90	22.09	23.32	5.18
Apparent density (g/cm^3)	0.336	0.420	0.555	0.609	0.796	0.884	0.933	0.207
Porosity (%)	81.51	80.57	79.05	78.45	76.34	76.22	75.31	84.01
Ligament thickness of Ni (μm)	141.23	111.94	153.18	144.91	205.77	246.91	263.31	0.00

Calculation Surface and volume of the network-solid by software: 2.19e+4 mm^2, 1440.57 mm^3 before electroforming. Apparent volume of all samples: 25 × 25 × 40 mm^3 and 6 PPI, Ni0: Cure resin without Ni coat 5.18 g, Ni density: 8.9 g/cm^3, Resin density: 1.21 g/cm^3, Total current: 33 Amps for all samples.

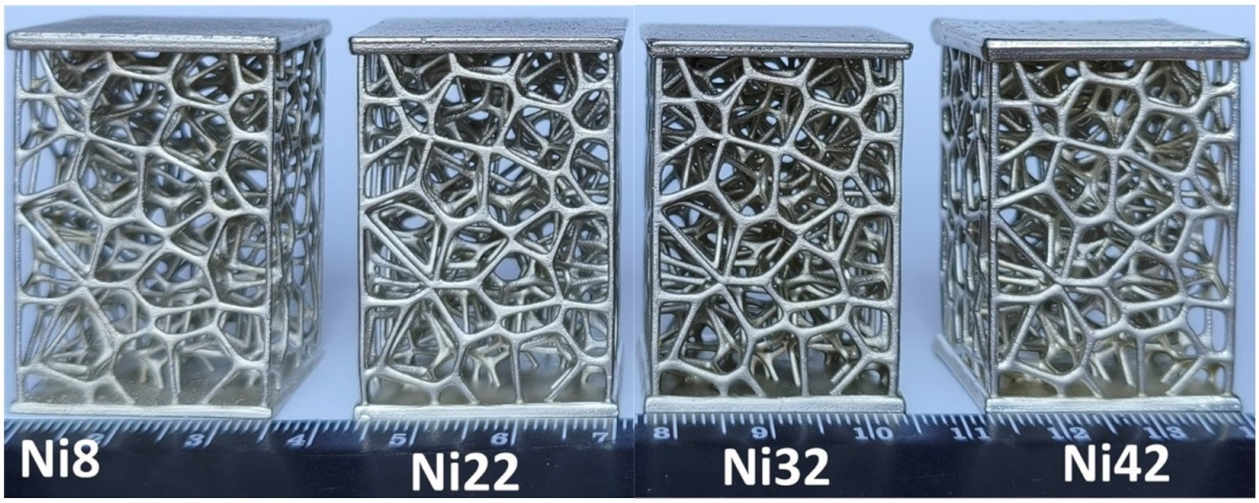

Fig. 2. Four samples on Ni open-cell structure according to data of Table 2.

Based on the deformation behavior illustrated in Figs. 3–6, the absence of ligament crumpling in Ni32 and Ni42 is attributed to their electroformed thickness, as reported in Table 2. It should be noted that the thickness of the electroformed Ni layer differs from the original ligament diameter. During electroforming, the resin ligaments with circular cross-sections were coated with a nickel ring. As shown in Fig. 7(a), several ligaments were extracted from the open-cell samples and mounted side by side for polishing. A single ligament was then magnified and schematically represented to illustrate the Ni ring and its thickness, as depicted in Fig. 7(b).

Assessment of the images in Figs. 3–6 shows that when the Ni electroformed thickness (Δx = dr) exceeds approximately 180–200 μm, ligament crushing and collapse are suppressed, and the deformation behavior of the Ni open-cell network transitions from brittle to ductile, accompanied by enhanced energy absorption. However, the assertion of increased plastic energy absorption and improved ductility at higher thicknesses must be verified by analyzing the force–displacement curves and the corresponding area under the curves up to the densification strain.

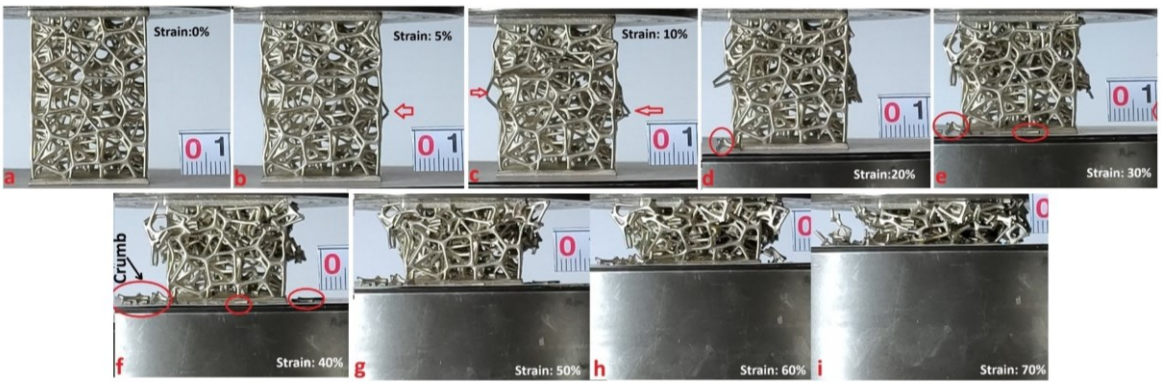

Fig. 3. Deformation behavior of the Ni8 sample with a thickness of 141 µm under strains from 0% to 70%. Red arrow showing local buckling of ligaments.

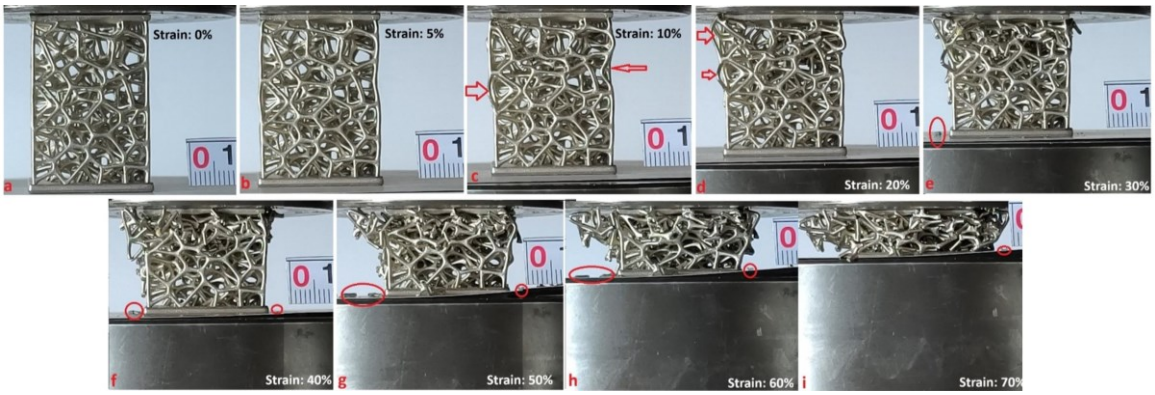

Fig. 4. Deformation behavior of the Ni22 sample with a thickness of 153 µm under strains from 0% to 70%. Red arrow showing local buckling of ligaments.

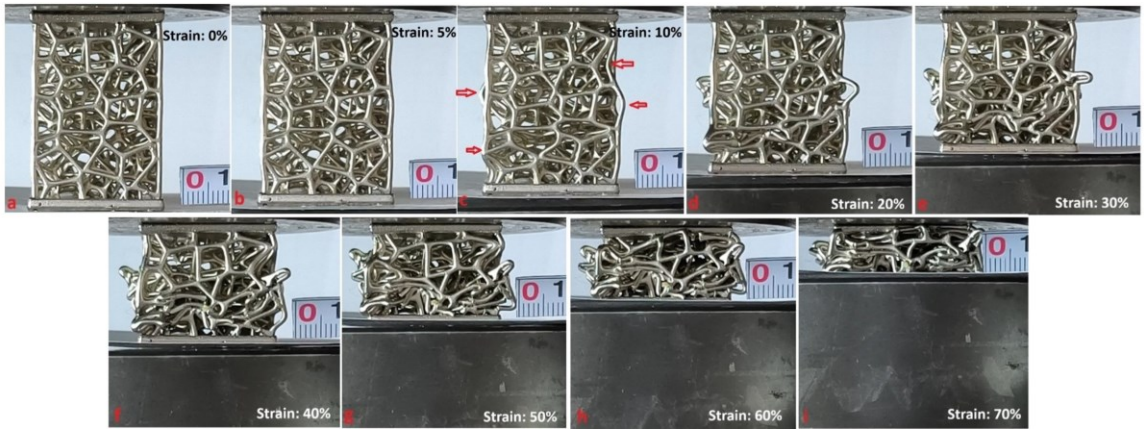

Fig. 5. Deformation behavior of the Ni32 sample with a thickness of 206 µm under strains from 0% to 70%. Red arrow showing local buckling of ligaments.

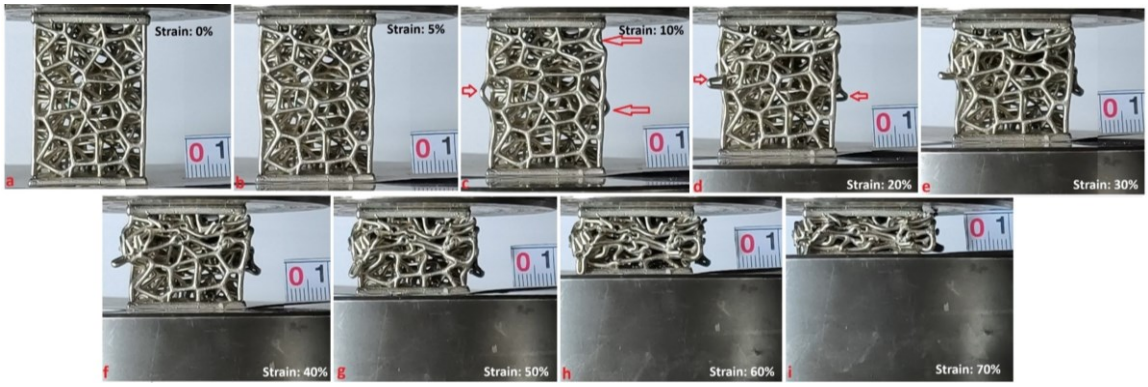

Fig. 6. Deformation behavior of the Ni42 sample with a thickness of 263 µm under strains from 0% to 70%. Red arrow showing local buckling of ligaments.

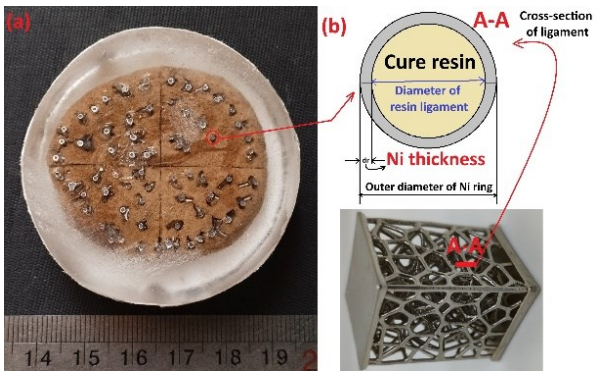

Fig. 7. Cross-sections of ligaments: (a) several ligaments mounted for polishing, (b) detailed view of a ligament cross-section after Ni electroforming.

3. Result and Discussion

Figs. 8–11 present the force–displacement curves, stress–strain responses, and energy absorption values at 50% and also 70% strain for the Ni8, Ni22, Ni32, and Ni42 samples, respectively. To better quantify the mechanical behavior under compressive plastic deformation, seven out of twenty open-cell nickel samples were selected, and their stress–strain curves were analyzed to extract the mechanical properties summarized in Table 3.

The results show that increasing the Ni ligament (ring) thickness enhances both strength and energy absorption. For example, when the thickness increases from 141.2 µm in the Ni8 sample to 264.9 µm in Ni42 sample, the first peak stress rises from 1.23 MPa to 7.56 MPa, while the energy absorption at 70% strain increases from 0.376 J·cm^{-3} to 4.998 J·cm^{-3}. Thus, a ~1.87-fold increase in nickel ring thickness results in up to a sixfold improvement in strength and a thirteenfold improvement in energy absorption at 70% strain.

Furthermore, when the mass of nickel within a fixed volume and pore size (25 cm^3, 6 PPI) increases from approximately 8.40 g to 23.32 g, the strength and energy absorption rise by factors of six and thirteen, respectively. However, this comparison can be more rigorously established by normalizing the mass and thickness with respect to the apparent density. As shown in Table 2, increasing the apparent density from 0.336 to 0.933 g/cm^3 results in this significant enhancement of mechanical properties. Comparisons of the first peak stress and the energy absorption at 50% and 70% strain for Ni8 to Ni42 samples are presented in Figs. 12 and 13, respectively.

In Fig. 14(a), the variation of mass during the warm electroforming process is presented. The increase in mass shows a linear relationship with electroforming time, which can be expressed by the following model:

$$m = 0.423\,t + 5.277 \quad (1)$$

where m is the mass of deposited nickel (g), and t is the electroforming time (h). Consequently, the variation of apparent density at a fixed volume (25 cm^3) and pore size (6 PPI) for the Ni open-cell samples is directly governed by the corresponding mass variation. As shown in Fig. 14(b), the apparent density variation correlates closely with the deposited mass over electroforming time. Furthermore, Fig. 14(c) presents the variation in nickel thickness with electroforming time, indicating that the overall deposition rate exhibits an increasing trend. This trend remains valid after excluding the 24-hour data point (highlighted in red in Fig. 14(c)), which was identified as erroneous due to a poor electrical connection during electroforming. Therefore, evaluating the mechanical properties of the Ni open-cell samples in terms of apparent density is both logical and more reliable, whereas expressing the mechanical properties with deposited mass thickness does not show a consistent correlation.

To validate this claim, several out of the twenty open-cell nickel samples were selected, as shown in Figs. 15, and their ligament cross-sections were examined under

Table 3. Physical and mechanical properties of Ni open-cell

Sample name /properties	Ni8	Ni14	Ni22	Ni28	Ni32	Ni34	Ni42	Ni0
Apparent density(g/cm^3)	0.336	0.420	0.555	0.609	0.796	0.884	0.933	0.207
First maximum stress (MPa)	1.230	1.972	3.512	3.496	5.898	7.184	7.559	0.16
Stress at 70% strain (MPa)	0.74	1.71	3.84	4.51	8.77	11.65	12.52	-
Density of energy at 70% strain (J/cm^3)	0.376	0.703	1.622	1.982	3.488	4.729	4.988	-
Density of energy at 50% strain (J/cm^3)	0.226	0.413	0.971	1.13	1.98	2.62	2.79	-

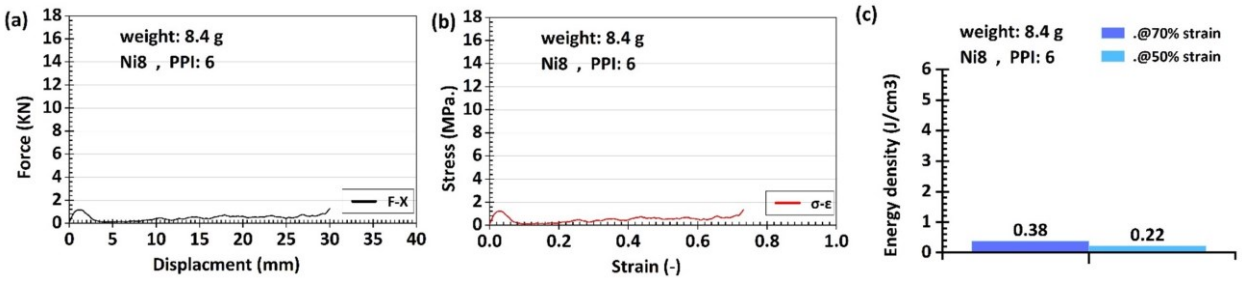

Fig. 8. Deformation behavior analysis of the Ni 8 sample: (a) force-displacement curve, (b) stress-strain curve, (c) absorption energy density.

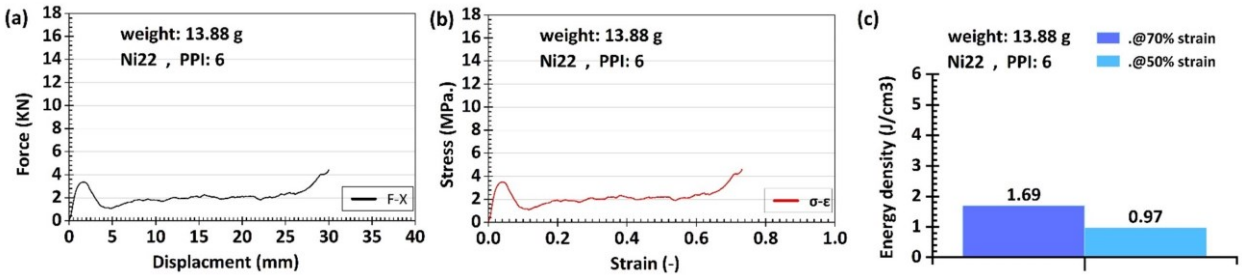

Fig. 9. Deformation behavior analysis of the Ni 22 sample: (a) force-displacement curve, (b) stress-strain curve, (c) absorption energy density.

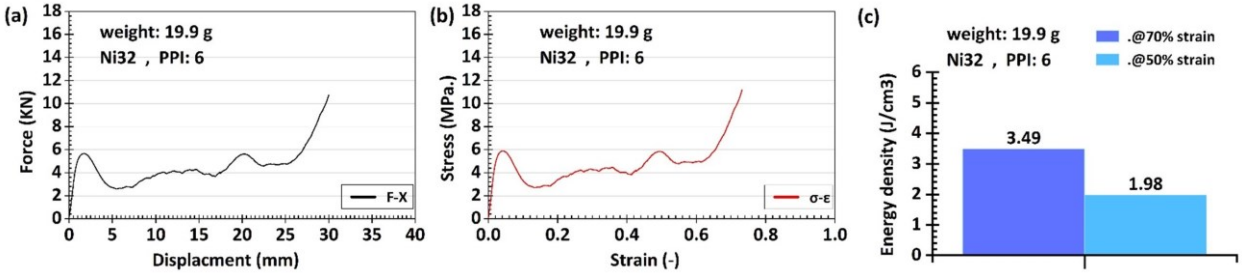

Fig. 10. Deformation behavior analysis of the Ni 32 sample: (a) force-displacement curve, (b) stress-strain curve, (c) absorption energy density.

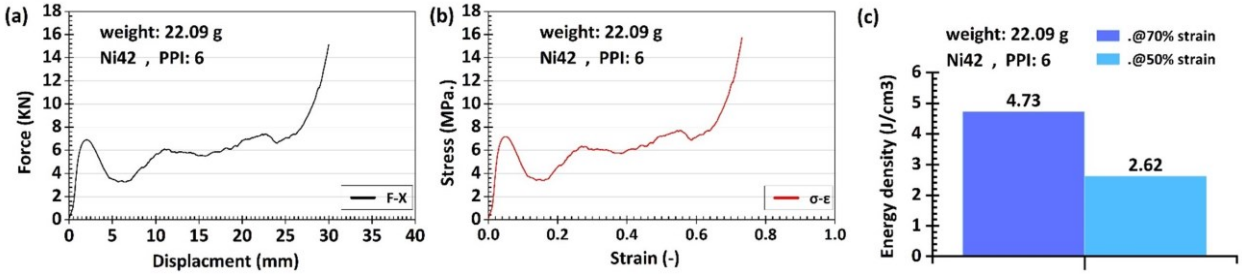

Fig. 11. Deformation behavior analysis of the Ni 42 sample: (a) force-displacement curve, (b) stress-strain curve, (c) absorption energy density.

an optical microscope after mounting and polishing. The images reveal that the resin ligaments were surrounded by a nickel ring, as also observed in the ligament cross-section shown in Fig. 7. To obtain an accurate average thickness of this metallic ring, approximately nine ligaments were extracted from each sample across a 25 × 25 mm cross-section, including both the outer surface and the core of the cubic samples. Eight thickness measurements were then taken around each ligament's ring ross-section, yielding a total of 81 measurements per sample. According to Fig. 16(a), the thickness variations of the seven cubic samples were plotted as a function of electroforming time. The results show that Ni thickness does not increase linearly with electroforming time. This behavior is attributed to the differences in Ni deposition between the core and outer surfaces of the cubic open-cell network, as well as between the nodes (ligament intersections) and the

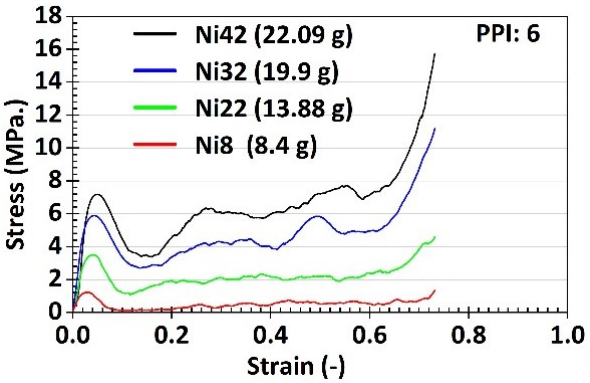

Fig. 12. Comparison of the stress-strain curves for Ni8 to Ni42 samples.

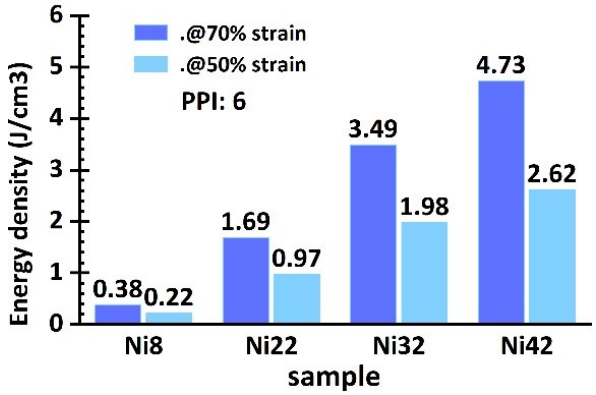

Fig. 13. Comparison of the energy absorption curves for Ni8 to Ni42 samples.

ligaments themselves. Moreover, as shown in Fig. 16(b), the mechanical properties, specifically the first maximum compressive stress (yield stress under compression) do not exhibit a consistent correlation with Ni thickness.

Therefore, comparing the mechanical properties with respect to the apparent density of the open-cell structures provides a more reliable basis than using either thickness or mass. Accordingly, all mechanical properties were plotted as a function of apparent density for the set of 20 samples, as shown in Figs. 17–18. According to ISO 13314, the standard test method for compressive properties of porous and cellular metals, the first maximum compressive strength (point 3 in Fig. 17(a)) was selected as the yield stress, or compressive resistance, for evaluating the strength of the Ni open-cell samples in this study. The results obtained from Fig.17(b), show that the variation of the the first maximum compressive stress with apparent density follows a liner trend. In addition, the area under the stress–strain curve up to 50% strain and 70% strain was calculated as a criterion for energy absorption during plastic compression for all 20 samples, as illustrated in Figs. 18(a) and 18(b).

As shown in Fig. 17(b), the compressive yield stress of the Ni open-cell samples increases with apparent density. This relationship can be expressed linearly as:

$$\sigma_c = 9.94\,\rho - 2.01 \qquad (2)$$

Where ρ is the apparent density (g/cm³) and σ_c is the compressive yield stress (MPa). The results obtained from this model show an error of 2–6%, which, according to Refs. [3, 13], is in good agreement with the predicted yield stress value for Ni open-cell structures having a pore size of 6 PPI.

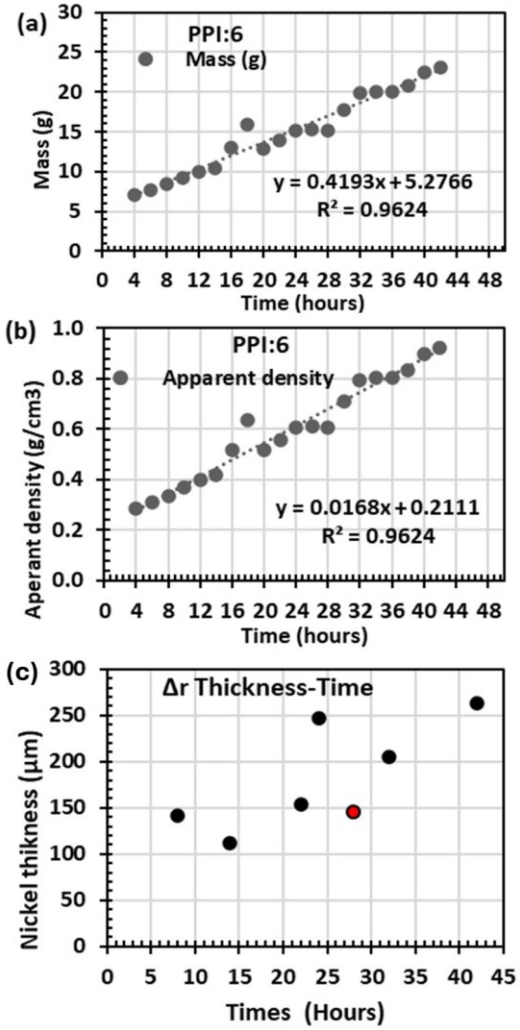

Fig. 14. (a) variation of mass during the electroforming as a liner equation, (b) variation of apparent density during the electroforming, (c) thickness of Ni via electroforming time.

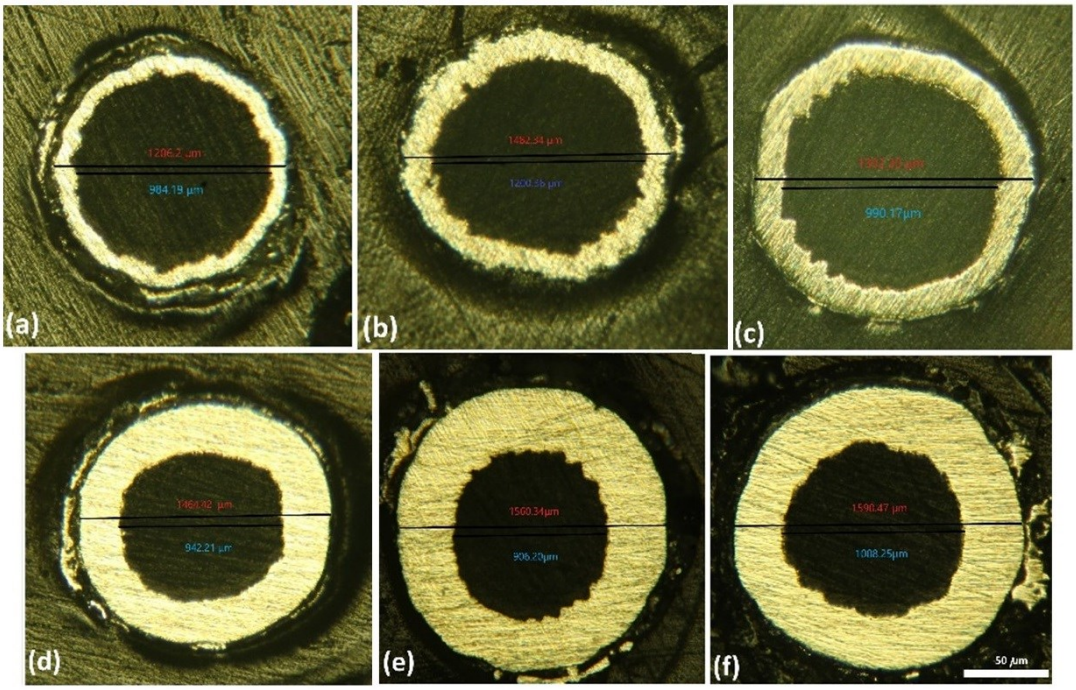

Fig. 15. Measurement of Ni-ring thickness for six samples: (a) Ni8, (b) Ni22, (c) Ni28, (d) Ni32, (e) Ni34, and (f) Ni42.

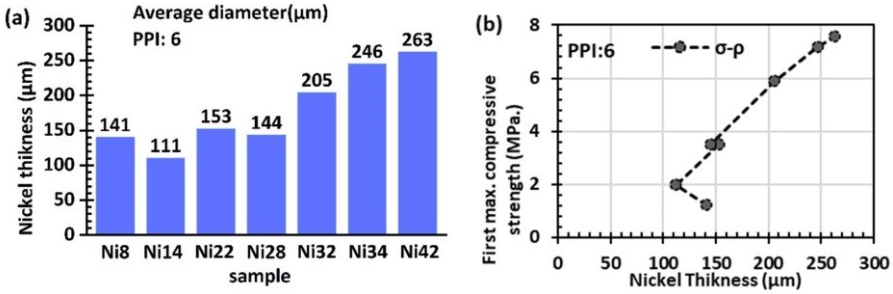

Fig. 16. (a) Variation of thickness with electroforming time, (b) nonlinear relationship between maximum compressive stress and nickel thickness.

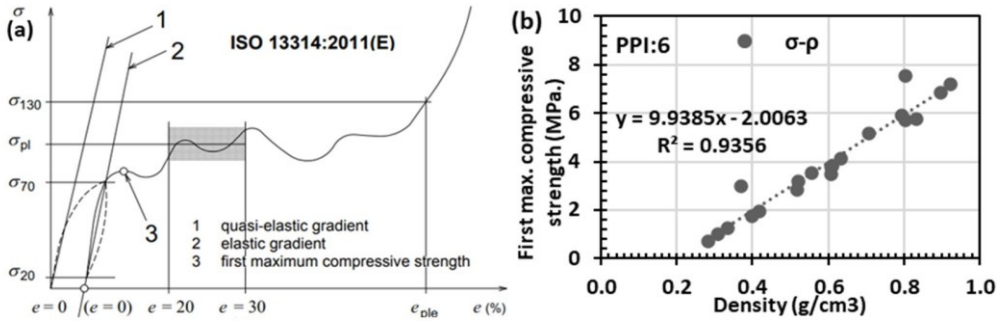

Fig. 17. (a) Definition of yield stress as point 3 according to ISO 14413 standard, (b) variation of the first maximum compressive stress with apparent density.

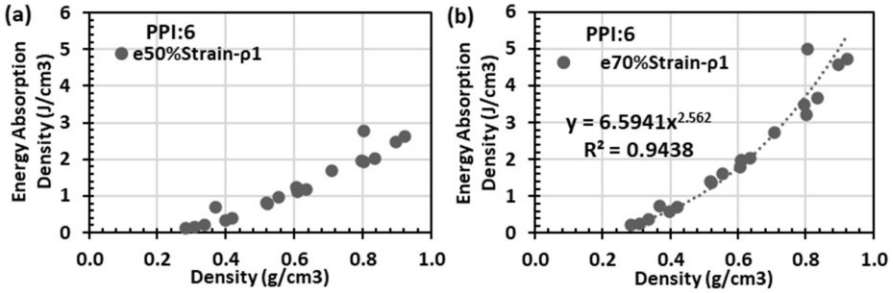

Fig. 18. Variation of the energy absorption via the apparent density: (a) at 50% strain, (b) at 70% strain.

However, as shown in Figs. 18(a–b), the variation of energy absorption density at 70% compressive deformation with apparent density (ρ_1) is better described by a power-law relationship, with an error of less than 2% for apparent densities below 0.65 g·cm^{-3} and less than 4% for higher apparent densities in the range of 0.65–1.0 g·cm^{-3}. The energy absorption behavior therefore be expressed by the following equation:

$$e_c = 6.5941\rho^{2.562} \quad (3)$$

In Eq. (3), e_c is the density of energy absorption (J/cm^3). In contrast, expressing energy absorption density as a function of Ni electroformed yields a significantly larger error of approximately 15–38%, indicating that apparent density is a more reliable predictor of mechanical performance. Therefore, the energy absorption behavior is considerably more sensitive to changes in apparent density than the compressive yield strength. Moreover, as shown in Fig. 18, the energy absorption values do not exhibit a linear correlation with apparent density. After the first peak corresponding to the maximum stress and the onset of foam structure collapse, the deformation stress level fluctuates depending on which ligaments—thick or thin, located in the core or near the outer surfaces—are hinged. The absorbed energy corresponds to the area under the force–displacement curves. Furthermore, the oscillations observed in the plateau region are irregular and do not follow a uniform pattern.

The mechanical properties corresponding to the first maximum compressive stress obtained in this investigation for several Ni open-cell structures are compared with Ashby's data [17] in Fig. 19 as a function of relative density. The yield compressive strengths of the Ni open-cell samples from Table 3 are shown by the black ellipse, while those reported by Ashby are shown by the red ellipse. As illustrated in Fig. 19(a), the yield strength of the Ni open-cell foams in this work is higher than those reported by Ashby and other researchers [18]. It is noticeable that the density of the cured resins was 1.22 g/cm^3, while that of Ni 8.98 g/cm^3 in the present work.

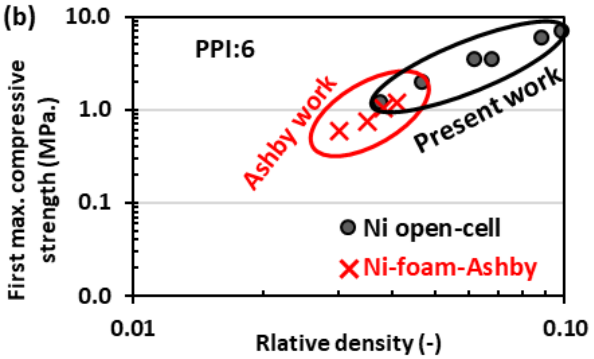

Fig. 19. Comparison of compressive strength between the present work (black ellipse, based on data from Table 3) and Ashby's data (red ellipses) for nickel foams. Ratio of resin to Ni is 1.22/8.98.

4. Conclusion

In this investigation, Ni open-cell structures were designed using CAD/CAM software and fabricated by combining SLA 3D printing, Ag electroless plating, and electroforming. Defect-free samples were successfully produced, and their mechanical and physical properties were systematically evaluated. The main findings are as follows:

1. All Ni open-cell structures with 6 PPI exhibited low apparent densities (<1 g·cm^{-3}).
2. When the Ni thickness exceeded approximately180–200 μm, ligament crushing and brittle fracture were suppressed, and the deformation behavior transitioned to ductile folding.
3. The first maximum compressive strength of Ni open-cell foams showed a linear dependence on mass or apparent density. However, no linear correlation was observed was observed with Ni thickness, due to the non-uniform distribution between the core and outer surfaces of the samples.
4. Energy absorption during compression up to 70% strain followed a power-law relationship with apparent density. This model remained consistent with the experimental results up to ~0.8 g·cm^{-3}, with an error of less than 2%.
5. For a Ni open-cell structure with a fixed volume (25 cm^3) and pore size (6 PPI), increasing the mass from 8.4 g to 23.3 g—corresponding to an increase in Ni thickness from 141 μm to 236 μm—resulted in an increase in energy absorption from 0.476 to 4.99

J·cm^{-3} and in yield compressive strength from 1.2 to 7.6 MPa. These represent improvements of approximately sixfold in strength and thirteenfold in energy absorption.

6. Comparison of compressive strength with Ashby's data for Ni open-cell foams indicates that the structures produced in this study exceed the strength and relative density limitations of Ashby's samples by more than 10 order of magnitude.

Acknowledgment

We gratefully acknowledge the support of *Rahyaft Advanced Sciences & Technologies*, a knowledge-based company, for their contribution to this academic project.

Authors' Contributions

J. Arta: Fabrication electroforming and Compressive test

S. Rohaninejad: Software, Designing and G-code

B. Yaghobzade: Image analyzer and measuring

S. M. H. Mirbagheri: Methodology, Project administration, Validation, Formal analysis; Writing-Original, Writing-review and editing

Conflict of interest

The author declares that there is no conflict of interest regarding the publication of this paper.

Funding

The author confirms that no funding was received from any institutions or organizations for this study.

5. References

[1] Hassan, A., & Alnaser, I. A. (2024). A review of different manufacturing methods of metallic foams. *ACS Omega*, *9*(6), 6280–6295. https://doi.org/10.1021/acsomega.3c08613

[2] Wang, L., He, L., Liu, F., Yuan, H., Li, J., & Chen, M. (2024). Mechanical characterization of multifunctional metal-coated polymer lattice structures. *Materials*, *17*(3), 741. https://doi.org/10.3390/ma17030741

[3] Rohani Nejad, S., Hosseinpour, M., & Mirbagheri, S. M. H. (2022). Investigation of energy absorption behavior of light sandwich panel with nickel/polymer open-cell foam core during compression. *Advanced Engineering Materials*, *24*(12), 1–13. https://doi.org/10.1002/adem.202200663

[4] Maconachie, T., Leary, M., Lozanovski, B., Zhang, X., Qian, M., Faruque, O., & Brandt, M. (2019). SLM lattice structures: Properties, performance, applications and challenges. *Materials and Design*, *183*, 108137. https://doi.org/10.1016/j.matdes.2019.108137

[5] Shajari, Y., & Nikzad, L. (2023). Investigation on mechanical properties of nickel open cell metal foam after heat treatment. *Scientific Reports*, 1–9. https://doi.org/10.1038/s41598-023-42857-w

[6] Badiche, X., Forest, S., Guibert, T., Bienvenu, Y., Bartout, J. D., Ienny, P., Croset, M., & Bernet, H. (2000). Mechanical properties and non-homogeneous deformation of open-cell nickel foams: application of the mechanics of cellular solids and of porous materials. *Materials Science and Engineering: A*, *289*(1-2), 276-288.

[7] McCullough, K. Y., Fleck, N. A., & Ashby, M. F. (1999). Uniaxial stress–strain behaviour of aluminium alloy foams. *Acta materialia*, *47*(8), 2323-2330.

[8] Gibson, L. J., & Ashby, M. F. (1997). *Cellular solids: structure and properties* (2nd ed.). Cambridge University Press.

[9] Aly, M. S. (2010). Tensile properties of open-cell nickel foams. *Materials & Design*, *31*(4), 2237–2240. https://doi.org/10.1016/j.matdes.2009.10.018

[10] Rohani Nejad, S., Hesari, S., & Mirbagheri, S. M. H. (2024). Effect of nickel and copper shells on mechanical properties of advanced lightweight TPU metamaterials during uniaxial compression. *Scientific Reports*, *14*(1), 1–16. https://doi.org/10.1038/s41598-024-82317-7

[11] Arnet, R., Kesten, O., El Mofid, W., & Sörgel, T. (2023). Combining 3d printing and electrochemical deposition for manufacturing tailor-made 3D nickel foams with highly competitive porosity and specific surface area density. *Metals*, *13*(5). https://doi.org/10.3390/met13050857

[12] He, L., Wang, P., Wang, L., Chen, M., Liu, H., & Li, J. (2023). Multifunctional polymer-metal lattice composites via hybrid additive manufacturing technology. *Micromachines*, *14*(12), 2191. https://doi.org/10.3390/mi14122191

[13] Wang, J., Berardi, P., Bártolo, P. J., Thompson, G. W., & Mahtabi, M. J. (2025). Electrodeposition of nickel onto polymers: a short review of plating processes and structural properties. *Applied Sciences*, *15*(15), 8500. https://doi.org/10.3390/app15158500

[14] Geng, X., Wang, M., & Hou, B. (2023). Experiment investigation of the compression behaviors of nickel-coated hybrid lattice structure with enhanced mechanical properties. *Micromachines*, *14*(10), 1959. https://doi.org/10.3390/mi14101959

[15] Besharati, F., & Paydar, M. H. (2023). Fabrication of copper open cell foam by electrochemical deposition method and investigation on the effect of current intensity and plating solution on the created microstructure. *Iranian Journal of Materials Forming*, *10*(1), 4-12. https://doi.org/10.22099/IJMF.2023.46551.1245

[16] SO 13314:2011. Mechanical testing of metals—Ductility testing—Compression test for porous and cellular metals. International Organization for Standardization, Geneva, Switzerland.

[17] Ashby, M. F., Evans, A., Fleck, N. A., Gibson, L. J., Hutchinson, J. W., Wadley, H. N. G., & Delale, F. (2001). Metal foams: a design guide. *Applied Mechanics Reviews*, *54*(6), B105-B106. https://doi.org/10.1016/B978-0-7506-7219-1.X5000-4

[18] Bauer, J., Hengsbach, S., Tesari, I., Schwaiger, R., & Kraft, O. (2014). High-strength cellular ceramic composites with 3D microarchitecture. *Proceedings of the National Academy of Sciences of the United States of America*, *111*(7), 2453–2458. https://doi.org/10.1073/pnas.1315147111